Bioconjugate Chemistry

Article

pubs.acs.org/bc

Radiolabeling of Poly(lactic-*co*-glycolic acid) (PLGA) Nanoparticles with Biotinylated F-18 Prosthetic Groups and Imaging of Their Delivery to the Brain with Positron Emission Tomography

Rachael W. Sirianni,[§,⊥] Ming-Qiang Zheng,[§] Toral R. Patel,[†] Thomas Shafbauer,[§] Jiangbing Zhou,[‡] W. Mark Saltzman,[‡] Richard E. Carson,[§,‡] and Yiyun Huang*[,§]

[§]PET Center, Department of Diagnostic Radiology, Yale University School of Medicine, New Haven, Connecticut 06510, United States

[†]Department of Neurosurgery, Yale University School of Medicine, New Haven, Connecticut 06511, United States

[‡]Department of Biomedical Engineering, Yale University, New Haven, Connecticut 06520, United States

[⊥]Barrow Neurological Institute, 350 West Thomas Rd, Phoenix, Arizona 85013, United States

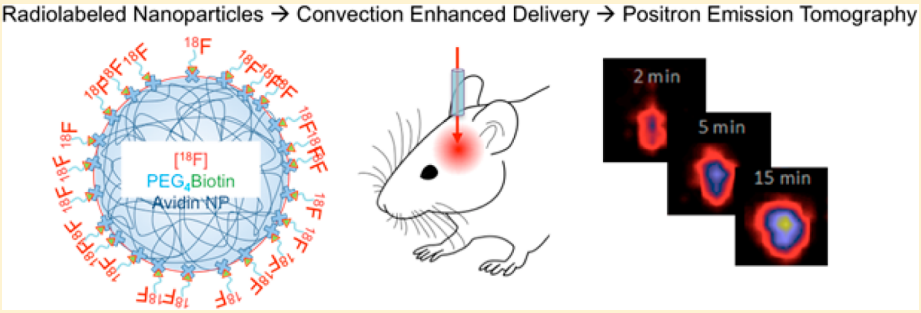

ABSTRACT: The avidin−biotin interaction permits rapid and nearly irreversible noncovalent linkage between biotinylated molecules and avidin-modified substrates. We designed a biotinylated radioligand intended for use in the detection of avidin-modified polymer nanoparticles in tissue with positron emission tomography (PET). Using an F-18 labeled prosthetic group, [^{18}F]4-fluorobenzylamine, and a commercially available biotin derivate, NHS-PEG$_4$-biotin, [^{18}F]-fluorobenzylamide-poly-(ethylene glycol)$_4$-biotin ([^{18}F]NPB4) was prepared with high purity and specific activity. The attachment of the [^{18}F]NPB4 radioligand to avidin-modified poly(lactic-*co*-glycolic acid) (PLGA) nanoparticles was tested by using PET imaging to measure the kinetics of convection-enhanced delivery (CED) of nanoparticles of varying size to the rat brain. PET imaging enabled the direct observation of nanoparticle delivery by measurement of the spatial volume of distribution of radiolabeled nanoparticles as a function of time, both during and after the infusion. This work thus validates new methods for radiolabeling PEG-biotin derivatives and also provides insight into the fate of nanoparticles that have been infused directly into the brain.

INTRODUCTION

The avidin−biotin system is one of the strongest noncovalent interactions known in nature.[1] Each 66 kDa avidin protein can bind up to four biotin molecules with a K_d of ~10^{-15} M, an interaction that is 1,000−1,000,000 times stronger than the association of an antibody with its specific ligand. The near irreversible maintenance of biotin's association with avidin under a range of physiological temperatures and pH makes this system a particularly attractive candidate for noncovalent labeling where stability is desired. Not surprisingly, the avidin−biotin interaction remains a powerful tool in biological research applications that include protein detection (Western blot, enzyme linked immune sorbent assay), protein enrichment (immunoprecipitation, coimmunoprecipitation), and tissue staining (immunofluorescence).

The avidin−biotin interaction has been used previously for surface modification of polymer nanoparticles for drug delivery.[2−4] In one strategy, avidin is covalently linked to a lipid moiety such as palmitic acid, which is then incorporated into the oil phase of an emulsion to form solid polymer nanoparticles.[5] This approach has been employed for the surface modification of nanoparticles with biotinylated polymers or ligands to mediate nanoparticle distribution in the body. For example, nanoparticles composed of poly(lactic-*co*-glycolic acid) (PLGA) and avidin−lipid conjugates have been surface modified with poly(ethylene glycol) (PEG) to improve tissue penetration, or with peptide and antibody ligands to enhance uptake and intracellular release of drug payload.[3,6,7] A range of therapeutic agents can be encapsulated within PLGA nanoparticles, including small molecules, proteins, and oligonucleotides. Encapsulated agents are protected from clearance and degradation in biological

Received: July 17, 2014
Revised: October 15, 2014
Published: October 16, 2014

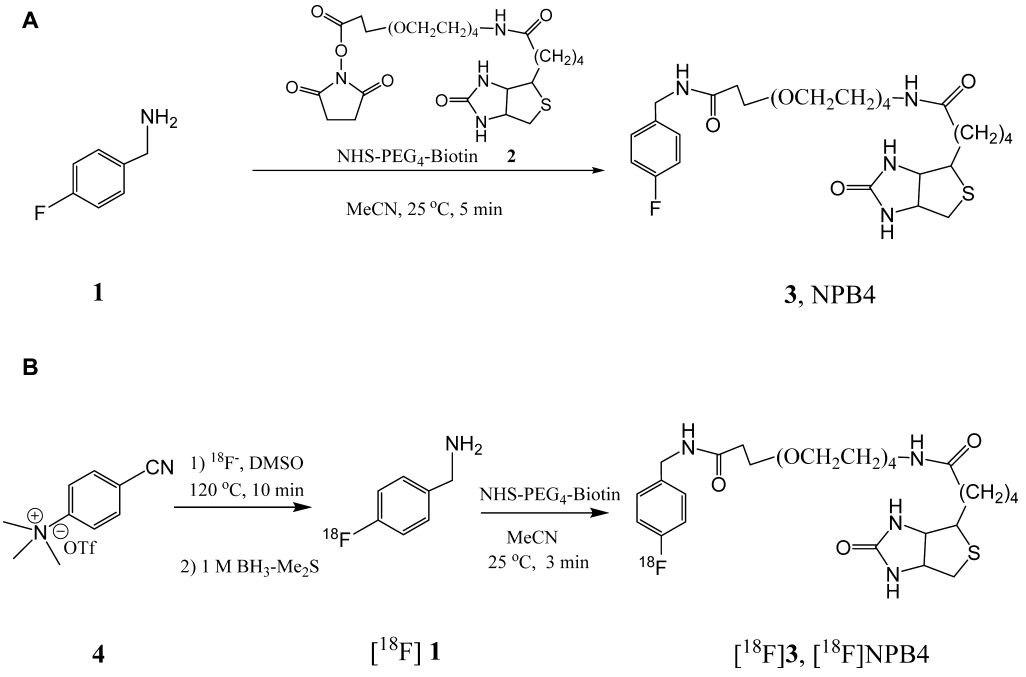

Figure 1. Synthesis of NPB4 (A) and [^{18}F]NPB4 (B).

environments, allowing agents to be released slowly by diffusion and as the polymer degrades by hydrolysis. Thus, when delivered directly to a tissue site, nanoparticles are capable of improving drug potency while reducing systemic exposure.

Drug-releasing nanoparticles have the potential to improve the treatment of diseases where prolonged drug action is required. For example, in prior work, we engineered PLGA nanoparticles to improve their penetration through brain extracellular matrix and delivered them directly to the brain via convection enhanced delivery (CED).[8] Nanoparticles that traveled farther were better able to improve the action of a novel chemotherapeutic agent, presumably because brain-penetrating nanoparticles enable the drug to reach a greater fraction of tumor cells. Direct injection methods such as CED are highly relevant to the development of new nanoparticle-based therapies to treat disease in the CNS,[9] and PLGA is a particularly interesting material candidate for the development of clinically relevant drug delivery systems, due to its long track record of safety in humans. To this end, PLGA microparticle formulations are clinically approved for use in humans for direct injection (e.g., Lupron Depot). Nanoparticles composed of PLGA have also been the focus of phase II clinical trials for targeted delivery of docetaxel in metastatic prostate cancer and nonsmall cell lung carcinoma (NCT01812746 and NCT01792479).[10,11]

The goal of this work was to develop a biotinylated radioligand to facilitate detection of avidin-modified polymer nanoparticles in tissue. Biotin has been labeled previously with radioactive isotopes such as Y-90, Ga-68, In-111, and Tc-99m.[12−15] Long-lived isotopes may be useful for measurements of nanoparticles with long bioavailability. However, since the kinetics of nanoparticle distribution in tissue is often rapid, on the order of minutes to hours, shorter-lived isotopes pose the advantage of lower total exposure to radiation. F-18 is likely to be a highly useful isotope for labeling agents intended for use in humans: its half-life of 110 min and decay by positron emission allow detection by positron emission tomography (PET), an imaging modality that possesses higher sensitivity and resolution than single photon emission computed tomography (SPECT).

Here, we describe a facile synthesis method for radiolabeling biotin derivatives to enable detection of polymer nanoparticles in intact tissue with PET. Using a well-developed F-18 labeled prosthetic group, [^{18}F]4-fluorobenzylamine, and commercially available biotin derivatives, NHS-PEGn-Biotin (n = 4, 12, etc.), radiolabeled PEGylated biotin, [^{18}F]-fluorobenzylamide-poly-(ethylene glycol)$_4$-biotin ([^{18}F]NPB4) was prepared with high purity and specific activity. These labeling methods are modular and could be used to modify PEG derivatives of varying length or with different end groups. [^{18}F]NPB4 was linked to avidin-modified PLGA nanoparticles to measure nanoparticle delivery in the intact brain of rats with PET.

RESULTS

Synthesis of [^{18}F]NPB4 and Its Conjugation with Avidin. We used a well-developed prosthetic group, [^{18}F]4-fluorobenzylamine ([^{18}F]**1**),[16−20] and a commercially available biotin derivate, NHS-PEG$_4$-Biotin, to prepare F-18 labeled PEGylated biotin ([^{18}F]**3**, i.e., [^{18}F]NPB4). The synthesis of NPB4 (**3**) and [^{18}F]NPB4 ([^{18}F]**3**) is shown in Figure 1. Total synthesis time for [^{18}F]NPB4 was 90 min, with a decay uncorrected overall radiochemical yield of 10 ± 8% (based on trapped [^{18}F]fluoride). The radiochemical purity of [^{18}F]NPB4 was 98.5 ± 1.2%, with specific activity of 3.5 ± 1.2 mCi/nmol (n = 10 batches, Figure 2A). To confirm the identity of the labeled compound, [^{18}F]NPB4 was coinjected with the nonradioactive reference compound NPB4 on an analytical HPLC system (Figure 2B). To confirm the integrity and the binding ability to avidin of the radiolabeled product, avidin was added to [^{18}F]NPB4 in an equimolar ratio of biotin in PBS solution and incubated for 5 min at room temperature. This solution was injected into a size-exclusion column; UV and radio-HPLC chromatography demonstrated a shift in peak

dx.doi.org/10.1021/bc500315j | Bioconjugate Chem. 2014, 25, 2157−2165

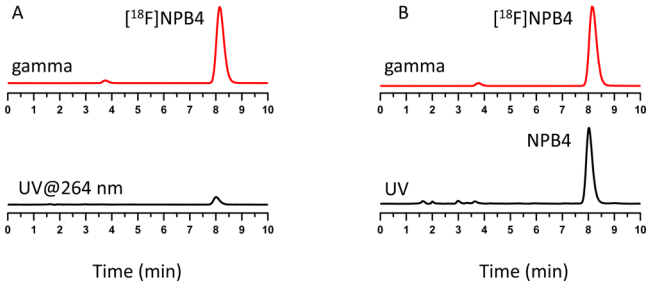

Figure 2. Analytical HPLC profile for [^{18}F]NPB4 solution. In (A), radiochemical purity of [^{18}F]NPB4 was 98.5 ± 1.2% (n = 10). In (B), the identity of [^{18}F]NPB4 was confirmed by its coelution with NPB4. Conditions: Phenomenex Luna C18 column (5 μm, 4.6 × 250 mm) eluted with 25:75 (v/v) acetonitrile/0.1 M ammonium formate with 0.5% acetic acid at a flow rate of 2 mL/min, wavelength set at 264 nm. Gamma (red) and UV (black) traces are shown. X-axis is time (min).

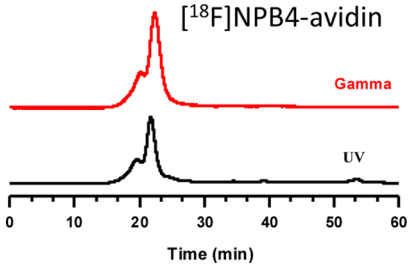

Figure 3. Analytical HPLC profile for the [^{18}F]NPB4-avidin complex. Near complete conjugation of [^{18}F]NPB4 to avidin was observed. Conditions: Superose 12, 10/300 GL column (10 ± 2 μm) eluted with 10% MeCN and 90% 0.1 M tris-HCl with 1 M NaCl at a flow rate of 0.8 mL/min, wavelength set at 254 nm. Gamma (red) and UV (black) traces are shown.

retention time from 37 to 22 min, which matched the retention time of the unlabeled NPB4-avidin standard (Figure 3). The recovery of radioactivity from the HPLC was 98%. The shoulder peak observed in the analytical HPLC profile is most likely due to dimer formation, as reported by others.[21]

Avidin-modified PLGA nanoparticles were prepared by single emulsion and size-fractionated via sequential centrifugation. The "large" fraction had an average diameter of 147 nm (±27 nm), whereas the "small" fraction had an average diameter of 71 nm (±13 nm) (Figure 4A, B), as measured by scanning electron microscopy. To confirm stable attachment of the radiolabeled biotin to avidinated nanoparticles, 5 mCi of [^{18}F]NPB4 was added to 20 mg/mL of large nanoparticles, sonicated for 30 min, and subjected to centrifugation (10,000 g for 10 min). No detectable amount of radioactivity remained in the supernatant, indicating complete attachment of [^{18}F]NPB4 to the nanoparticles.

We previously reported methods for using positron emission tomography (PET) to measure the distribution of radiotracers that were directly delivered to the rat brain or brain phantom.[22] Here, similar methods were applied to monitor the delivery and elimination of radiolabeled nanoparticles in the rat brain. Rats received a guide cannula, within which an internal injector was threaded to target infusions to the striatum. This enabled continuous imaging while nanoparticle infusions were ongoing. The infusion location was confirmed for each rat by identifying the surface of the skull in the PET transmission image and comparing to the location of the center of the nanoparticle infusion in the first or second frame (Figure 4C).

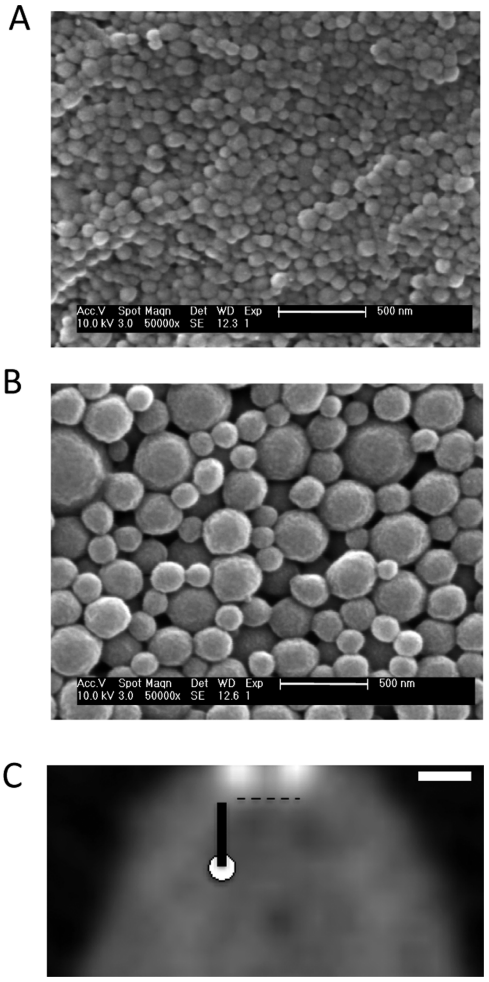

Figure 4. PLGA nanoparticles were prepared for delivery to the rat striatum. SEM images of small and large nanoparticle fractions are shown in (A) and (B), respectively. (C) A guide cannula was implanted to enable insertion of an internal injector for imaging while the infusion was ongoing. The injection location for each rat was verified by comparing the location of the surface of the skull (identified in the transmission image) with the center of the infusion (identified in the first several frames of the emission image). Scale bars: 500 nm (A,B), 5 mm (C).

Nanoparticles were delivered to the striatum via convection enhanced delivery (CED), a method that generates a positive pressure gradient to infuse fluid directly into the brain. The goal of CED is to generate convective forces to facilitate flow of drugs, drug carriers, or tracers (in this case, radiolabeled nanoparticles) through the relatively tight extracellular space of the brain. Nanoparticle distributions measured by PET were generally spherical (Figure 5A), with a spatial volume of distribution that increased throughout the infusion period (Figure 5B). As previously reported,[8] small nanoparticles achieved a greater V_d/V_i than large nanoparticles (5.50 ± 0.403, n = 3, and 2.83 ± 1.57, n = 2, for small and large nanoparticles, respectively; p = 0.0284, Student's one tailed t test). The spatial volume of distribution increased evenly with time for 2 of the 3 small nanoparticle infusions. In the third infusion, nanoparticles were not observed to distribute in the brain until 8 min after the infusion was initiated, after which the spatial volume of distribution increased evenly. The resultant profile was still spherical (data not shown). The final volume of distribution was similar for each of the 3 small nanoparticle

dx.doi.org/10.1021/bc500315j | Bioconjugate Chem. 2014, 25, 2157−2165

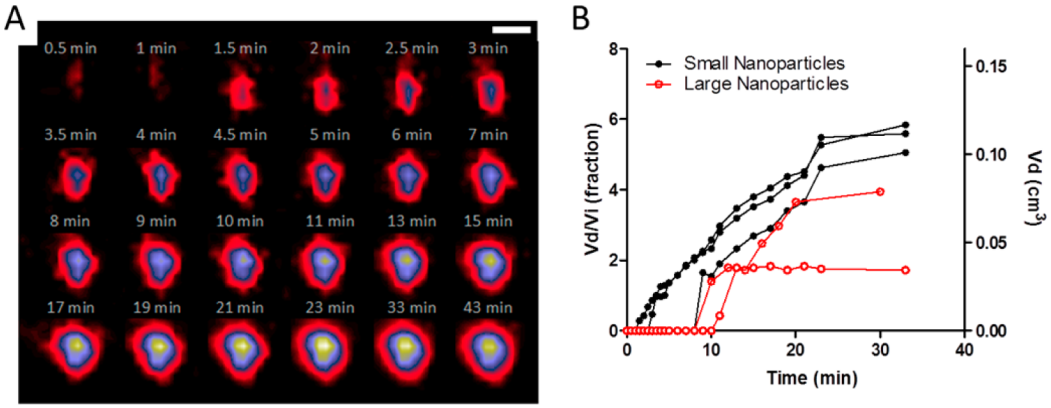

Figure 5. Spatial distribution of nanoparticles delivered to the brain via CED was measured with PET. An infusion volume of 20 μL was delivered over 30 min to the striatum. In (A), the spatial volume of distribution (V_d) of labeled nanoparticles is shown for a single subject that received small nanoparticles. Coronal images are shown in the direction parallel to the infusion track, and the scale bar is 5 mm. In (B), the ratio of V_d to the infusion volume (V_i) is plotted for 5 representative infusions.

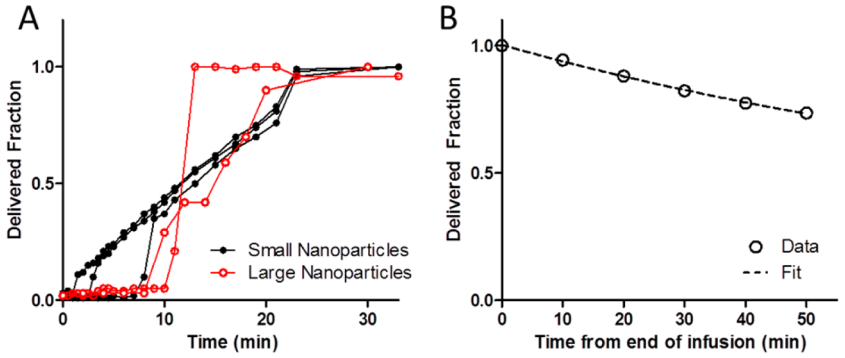

Figure 6. Kinetics of nanoparticle delivery and subsequent clearance were measured by PET. In (A), the total fraction of nanoparticles delivered to the brain was measured over 30 min. Small nanoparticles were delivered steadily, with total activity that increased smoothly and reproducibly over time. However, large nanoparticles were not delivered smoothly. Noncontinuous jumps in the total delivered fraction were observed at various points during the infusion. Once the infusion was complete, total radioactivity decreased. Representative data for a small nanoparticle infusion are shown in (B). Clearance half-life of the radioactive signal was calculated by fitting these data to a first order elimination model (111 min in this example).

infusions, whereas the spatial volume of distribution for large nanoparticles increased unevenly for both subjects, with large variability observed in the final volume of distribution (Figure 5B).

We quantified delivery kinetics by tracking the total radioactivity in the brain. Total signal in the brain increased during the infusion (Figure 6A). After the infusion was complete, total radioactivity decreased with time (Figure 6B). Elimination rates were estimated by fitting the data for radioactivity decrease over time to a first-order elimination model, yielding early tissue half-lives of 102 ± 6 min and 258 ± 66 min for small (n = 4) and large (n = 2) nanoparticle fractions, respectively (p = 0.0029 Student's one-tailed t test). Fitting the data to a two-phase model of elimination yields a tissue half-life for each phase (slow and fast): $t_{1/2,slow}$ = 36 min and $t_{1/2,fast}$ = 22 min. The two-phase model did not improve the absolute sum of squares compared to the one-phase model (6.1×10^{-5} versus 3.3×10^{-4}, respectively). It is important to note that half-lives calculated here represent early clearance rates, and there may be a fraction of nanoparticles bound to or internalized by cells that will be cleared at different rates over longer time periods.

DISCUSSION

The goal of this work was to develop methods for labeling polymeric nanoparticles with an F-18-biotin derivative to enable imaging of their delivery to intact tissue with PET. The first F-18 labeled biotin, reported in 1993, was produced by the reaction of [^{18}F]fluorobenzyl bromide and biotin-LC-hydrazide, a commercially available biotin derivative.[23] After radiolabeling with F-18, the amide-derivative of biotin maintained its binding affinity with avidin, highlighting its potential use for imaging of avidin−biotin linked agents. No further application of this compound in animal studies was reported, possibly due to its low labeling yield (5−10%) before HPLC purification. Shoup et al. modified the carboxylic acid chain on the biotin with an alkyl group for subsequent labeling with F-18.[24] However, this modification severely reduced the binding affinity of the modified biotin for avidin. Simplification of the synthesis route was achieved by Ting's group, using aryltrifluoroborate modified biotin derivatives.[25] Radiofluorination was achieved by F-18 for F-19 exchange in only one step, which is an advantage over the prior multistep approach, although the specific activity of the final product is expected to be low. Our synthesis method offers several advantages over prior approaches. First, the synthesis achieved high purity (98.5 ± 1.2%) and high specific activity (3.5 ± 1.2 mCi/nmol, n = 10 syntheses). Second, by attaching the radiolabel to a short

dx.doi.org/10.1021/bc500315j | Bioconjugate Chem. 2014, 25, 2157−2165

biotin-PEG linker, additional modification of biotin is avoided, thus preserving functionality for its attachment to avidin. Third, the PEG linker facilitates modular chemistry, with varying lengths of the PEG unit between biotin and the prosthetic group. This scheme could also be adapted to modify PEG linkers with nonbiotin end groups.

Avidin-modified nanoparticles were labeled with [^{18}F]NPB4 and delivered to the rat brain for imaging with PET. We have explored the functional ligand-binding efficiency of avidin-modified nanoparticles in other work.[5] Assuming a PLGA density of 1.25 mg/cm^3 and complete incorporation of avidin, and calculating across the range of specific activities and delivered doses presented for these in vivo experiments, we estimate that each small nanoparticle binds at least 5 and up to 80 [^{18}F]NPB4 molecules. For a typical experiment (e.g., 0.1 mCi delivered with a specific activity of 5 mCi/nmol), [^{18}F]NPB4 molecules would occupy 1.3% of biotin-binding sites that are available for each nanoparticle. Radiolabeled nanoparticles were delivered effectively to the brain with CED, as evidenced by an increase in the spatial volume of distribution of the signal over time. Nanoparticles reached a final V_d/V_i that was a function of nanoparticle size and consistent with prior measurements made by fluorescence imaging.

CED of nanoparticles was well-tolerated by all experimental subjects, and we observed no reactions to the nanoparticles in these or other studies. However, one concern regarding application of these methods in human subjects is the potential for avidin to be immunogenic. Although avidin is capable of generating an immune response in humans, interestingly, the presence of antiavidin antibodies does not interfere with the therapeutic use of avidin protein.[26] For example, Grana et al. observed that although patients developed anti-avidin antibodies while undergoing radioimmunotherapy, the treatment was reported to be well-tolerated with no acute or subacute side effects.[27] Similarly, Petronzelli et al. examined the avidin-induced immunological response of human oncology patients and mice with high anti-avidin antibody levels and determined that the anti-avidin antibodies did not affect the safety or efficacy of avidin formulations.[28] Lastly, we note that alternative biotin-binding proteins with reduced immunogenic potential (e.g., streptavidin) could also be used to modify the surface of nanoparticles.

The delivery of nanoparticles was tracked in real time by monitoring total activity in the brain, which increased during the first 30 min, as nanoparticles were infused, and decreased thereafter. Small nanoparticles were infused smoothly once they entered the brain, and the total delivered fraction increased to achieve a final volume of distribution that was similar in each of the three subjects tested. However, when large nanoparticles were delivered by the same protocol, the spatial volume of distribution and total delivered radioactivity increased unevenly as a function of time to achieve a variable final volume of distribution.

Noncontinuous jumps in the volume of distribution and total delivered activity were observed for nanoparticles (Figures 5 and 6); this pattern in the infusion data was not observed in any of our prior studies involving infusion of free and bound radiotracer solutions (including free fluoride ion, [^{18}F]NPB4 and [^{18}F]NPB4-avidin) into the brain with the same cannulation and CED protocol. There are several possible explanations for the lack of continuity observed for these nanoparticle infusions. Nanoparticles could exit the infusion needle unevenly, tissue could enter the needle during its placement so that nanoparticles are not able to circumnavigate the plug, or the extracellular space of the brain could become crowded with nanoparticles in a manner that halts additional fluid entry into the brain. These observations, which reflect potential delivery barriers that are apparently unique to the nanoparticle infusions, could not have been made using conventional fluorescence-based imaging techniques, and thus highlight the utility of PET imaging for monitoring drug delivery effectiveness.

The total decay-corrected activity in the brain increased during the infusion period and decreased once the infusion was complete. Early tissue clearance half-life of total radioactivity in the brain was estimated from the elimination data and found to be a function of the size of nanoparticles that were infused (102 and 258 min for small and large nanoparticles, respectively). In prior work, [^{18}F]fluoride ion and [^{18}F]NPB4 were delivered to the brain by similar methods, yielding tissue clearance half-lives of 41 and 19 min for free [^{18}F]fluoride ion and [^{18}F]NPB4, respectively.[22] Loss of radiotracer was therefore a function of both the attachment of the tracer to the nanoparticle as well as the size of the nanoparticle itself.

Total radioactivity in the brain decreased after the infusion was halted (30% loss after approximately 1 h for small nanoparticles). Loss of radioactivity from the brain could represent one of two phenomena: either radioligand (in the form of free fluoride ion, intact [^{18}F]NPB4, or the [^{18}F]NPB4-avidin complex) is liberated from the surface of the nanoparticle and this free tracer is subsequently cleared from the brain, or the intact nanoparticle exits the brain with the radiolabel attached. In our prior work, [^{18}F]NPB4 and [^{18}F]NPB4-avidin were also infused into agarose gels, and the diffusion of radiotracers was observed by PET imaging over several hours.[22] The data were analyzed by quantitative modeling, and a significant reduction in the diffusion coefficient was found after conjugation to avidin, from 0.022 ± 0.003 to 0.004 ± 0.002 mm^2/min; this reduction in diffusion coefficient is consistent with an increase in molecular weight resulting from attachment of the [^{18}F]NPB4 (0.5 kDa) radiolabel on avidin (66 kDa). Given these prior data, as well as the extremely high affinity of avidin for biotin (10^{-15} M), we expect that biotinylated tracer will not be released from avidin, even in vivo. Such an expectation is supported by experimental data from the literature. For example, it was reported that replacement of fluorescently labeled biotin from avidin by unlabeled biotin was extremely slow, occurring over a time scale of days.[29] In other studies, incubation of streptavidin attached to a biotinylated peptide with ∼50 mM of D-biotin for 1 h failed to dissociate the biotinylated peptide.[30] Since endogenous biotin levels are low (∼10 nM in mouse),[31] it is unlikely that substantial displacement of [^{18}F]NPB4 from avidin by endogenous biotin would occur in vivo over the time scale of interest for our experiments.

The association of the [^{18}F]NPB4-avidin palmitate complex with nanoparticle is noncovalent, and so one important question is whether the intact radioligand remains securely attached to the nanoparticle. In this study, the attachment of radioligand to nanoparticles was highly stable in aqueous conditions over the course of an hour, which confirms prior work demonstrating 2−6% loss of avidin conjugate or biotinylated ligand from the surface of PLGA nanoparticles in 1 h under physiological conditions.[6] We also observed dramatically different elimination half-lives for free versus nanoparticle-bound radioligand (19 min versus 102 and 258

dx.doi.org/10.1021/bc500315j | Bioconjugate Chem. 2014, 25, 2157−2165

min for small and large nanoparticles, respectively[22]). If the loss of radioactivity reflected unstable attachment of radiolabel to nanoparticles in vivo, we would expect the elimination curves to be governed by two kinetic processes (first, liberation of the radiolabel, and, second, brain clearance of the liberated radiolabel). However, a two-phase decay model did not improve the quality of data fit over a one-phase model. The kinetic data therefore provides no suggestion of radiolabel detachment from the nanoparticle. We speculate that the different early tissue half-lives measured for small and large nanoparticles reflect underlying differences in the residence of these nanoparticles in tissue.

In this work, we present a novel method for radiolabeling PLGA nanoparticles with a biotinylated F-18 prosthetic group. [^{18}F]NPB4 was prepared with high purity and high specific activity. Radiolabeled nanoparticles were delivered to the brain by CED and imaged with PET. The final spatial volume of distribution measured by PET is in accordance with prior work measuring nanoparticle distributions by fluorescence. Dynamic measurement of spatial volume of distribution and total radioactivity in the brain revealed transient discontinuities in the rate that nanoparticles reached the brain. Once the infusion was complete, total radioactivity in the brain decreased as a function of nanoparticle size. These data suggest that nanoparticles may encounter additional barriers to direct delivery to the brain by CED that are not encountered by free molecules, and further motivate the use of quantitative imaging techniques in the development of novel drug delivery systems.

EXPERIMENTAL PROCEDURES (MATERIALS AND METHODS)

Reagents. All reagents used were commercial products purchased from Sigma-Aldrich or Fluka and were used without further purification, unless otherwise indicated. O-18 water (98% pure) was purchased from Huayi Isotopes Co. (Toronto, Canada). EZ-link NHS-PEG$_n$-Biotin (n = 4 (**2**) or 12) was purchased from Thermo Scientific. Avidin was purchased from Fisher Scientific Company LLC. A Superose 12 column (10/300 GL) was purchased from GE Healthcare Life Sciences. Chromafix 30-PS-HCO$_3$ was purchased from Macherey-Nagel. Flash chromatography was carried out with silica gel 60 (200−400 mesh). ^{1}H spectra were recorded on a Bruker spectrometer at 500 MHz. Chemical shifts are reported in parts per million (ppm). Coupling constants are reported in hertz (Hz). High resolution mass spectroscopy (HRMS) was carried out on a Bruker 9.4T FT-ICR MS spectrometer. Purification of [^{18}F]NPB4 was done by reverse phase semipreparative HPLC using a Phenomenex Luna C18(2) ODS(3) column (10 μm, 10 × 250 mm), eluting at a flow rate of 5 mL/min under isocratic conditions with a mobile phase composed of 24:76 (v/v) acetonitrile/0.1 M ammonium formate solution with 0.5% acetic acid (pH = 4.2). Quality control analyses were carried out using a Shimadzu LC-20AT Prominence HPLC system equipped with an SPD-M20A photo diode array detector or an SPD-20A UV/vis detector (264 nm) operating in series with a Bioscan Flow-Count gamma detector (HPLC column: Phenomenex Luna C18, 5 μm, 4.6 × 250 mm; mobile phase: 25:75 (v/v) acetonitrile/0.1 M ammonium formate with 0.5% acetic acid (pH = 4.2); flow rate: 2 mL/min).

Synthesis of 4-Cyano-*N,N,N*-trimethylanilinium Trifluoromethanesulfonate (4). 4-(Dimethylamino)-benzonitrile (5 g, 34 mmol) and methyl trifluoromethanesulfonate (10 g, 60.9 mmol) were dissolved in CH_2Cl_2 (100 mL) and the reaction mixture stirred at room temperature under argon overnight. The resulting precipitate was filtered and washed with EtOAc. The solid was then redissolved in MeOH (10 mL) while heating and EtOAC was added to crystallize. The crystal was collected and recrystallized in MeOH (4 mL) and EtOAc to give compound **4** as yellow flakes (6.4 g, 60.7%), mp 156−158 °C (lit. 156−158 °C.[32] ^{1}H NMR (500 MHz, DMSO-d_6): δ 8.21 (b, 4H), 3.65 (s, 9H).

Synthesis of Fluorobenzylamide-poly(ethylene glycol)$_4$-biotin (3, NPB4). 4-Fluorobenzylamine (200 μL, 125 μmol) was dissolved in CH_3CN (5 mL) and mixed with EZ-link NHS-PEG$_4$-biotin (205.5 mg, 0.35 μmol). The reaction mixture was stirred for 5 min at room temperature. The precipitate was removed by filtration and the filtrate concentrated with rotary vacuum evaporator. The residue was dissolved in MeOH (1 mL) and purified by flash chromatography on silica gel (0% to 50% MeOH in CH_2Cl_2) to give **3** as colorless oil (54 mg, 25.7%). ^{1}H NMR (500 MHz, DMSO-d_6): δ 8.33 (m, 1H), 7.80 (m, 1H), 7.30−7.15 (m, 2H), 7.09 (t, J = 8.8, 2H), 6.40−6.30 (m, 2H), 4.21 (m, 2H), 4.20 (m, 2H), 4.07 (m, 1H), 3.58 (t, J = 6.3, 2H), 3.50−3.45 (m, 12H), 3.16−3.11 (m, 3H), 2.88−2.66 (m, 2H), 2.33 (m, 3H), 2.01 (t, J = 7.4, 2H), 1.62−1.20 (m, 6H). HRMS: calculated for $C_{28}H_{43}FN_4O_7S$ $[M+1]^+$: 599.2909; found 599.2896. The purity of NPB4 was greater than 98% based on the analysis with HPLC.

Synthesis and Characterization of [^{18}F]-fluorobenzylamide-PEG$_4$-Biotin ([^{18}F]3, [^{18}F]NPB4). No-carrier-added aqueous [^{18}F]fluoride was produced in a GE PETtrace cyclotron via ^{18}O(p, n)^{18}F nuclear reaction and transferred to a lead-shielded hot cell. The [^{18}F]fluoride ion was trapped on a Chromafix 30-PS-HCO$_3$ cartridge, and then eluted to a V-vial (2 mL) with a solution of Kryptofix −222 (10 mg) and K_2CO_3 (1.04 mg) in 1.4 mL of MeCN/H_2O (1:0.4, v/v). The solvent is subsequently evaporated at 105 °C under a stream of inert gas, and followed by addition of two portions of MeCN (0.4 mL each) for azeotropic removal of water under the same inert gas flow. 4-*N,N,N*-Trimethylammonium benzonitrile triflate **4** (7 mg) in anhydrous DMSO (0.2 mL) was then added to the above vial containing dried [^{18}F]fluoride. The mixture was heated at 120 °C for 10 min. After cooling down, a solution of 1 N borane-dimethylsulfide complex in THF (0.2 mL) was added to the vial and the reaction mixture kept at room temperature for 5 min to generate the radioactive intermediate, [^{18}F]4-fluorobenzylamine ([^{18}**F**]**1**). The solvent was removed at 60 °C and the reaction quenched with addition of 5 N HCl solution (2 mL). The solution was transferred to a bottle with deionized (DI) water (5 mL) and 1 N NaOH (12 mL) and the mixture passed through two Waters Classic C18 SepPak cartridges in series. The cartridges were washed with DI water (10 mL). The intermediate was then eluted off with 1 mL of MeCN into a vial preloaded with the NHS-PEG$_4$-Biotin powder (3−5 mg) and mixed for 3 min to yield the product [^{18}F]**3** ([^{18}F]NPB4). The volume in the vial was reduced to ∼0.5 mL by heating at 80 °C under a stream of nitrogen, diluted with DI water (1.5 mL), then loaded onto the semipreparative HPLC system for further purification. The fraction corresponding to the product (retention time of ∼18 min) was collected in a dilution bottle containing 50 mL of DI water, and the solution passed through a Waters Classic C18 SepPak cartridge. The SepPak was rinsed with 0.001 N HCl (10 mL) and dried with air. The product was then eluted off the SepPak with 1 mL of MeOH. The solvent was evaporated

at 80 °C under a stream of nitrogen and the residue was redissolved in an appropriate amount of phosphate buffer solution (PBS, pH = 7.4) for use in conjugation with nanoparticles. A sample of the product in PBS was injected to the analytical HPLC system to determine the radiochemical purity and specific activity of the product. Specific activity was determined by counting an aliquot of the product in a dose calibrator for radioactivity amount and performing HPLC analysis of the aliquot. The mass of NPB4 associated with the injection was measured by comparing the corresponding UV area with a standard curve relating UV area with mass.

Synthesis and Characterization of [^{18}F]NPB4-avidin. Avidin (0.66 mg, 10 nmol) was added to the solution of [^{18}F]NPB4 in PBS (3−4 mCi, 1 mL, ∼1 nmol) and the solution incubated for 5 min at room temperature. A small sample of [^{18}F]NPB4 PBS solution (free [^{18}F]NPB4) and the mixture of [^{18}F]NPB4-avidin were coinjected to the size-exclusion column (Superose 12, 10/300 GL column, 10 ± 2 μm) eluting with a mobile phase of 10% MeCN and 90% 0.1 M tris-HCl with 1 M NaCl at a flow rate of 0.8 mL/min. The retention times were 22 and 37 min, respectively, for [^{18}F]NPB4-avidin conjugate and free [^{18}F]NPB4. HPLC eluent was collected in fractions. Radioactivity in the fractions was measured and decay-corrected to the injection time. The recovery of radioactivity from HPLC was 98%, indicating the elution of all injected radioactivity from the column. A separate injection of the reaction solution detected no presence of the free [^{18}F]NPB4 peak on the chromatogram, demonstrating complete conjugation of [^{18}F]NPB4 with avidin.

Nanoparticles. Avidin-palmitate was prepared by reacting avidin protein (25 mg) with palmitic acid *N*-hydroxysuccinimide ester (1 mg) in 2% sodium deoxycholate buffer (NaDC, 5 mL) at 37 °C overnight. The resulting product was dialyzed against 0.3% NaDC to remove unreacted products. Nanoparticles encapsulating the hydrophobic dye coumarin-6 (C6) were prepared by single emulsion.[33] Briefly, 100 mg of PLGA (Durect, Lactel) was dissolved with 1 mg C6 in 2 mL ethyl acetate. The organic phase was added dropwise to 4 mL of water containing the stabilizer poly(vinyl alcohol) (PVA, 2.5 wt %) and the fatty acid conjugate avidin-palmitate (5 mg) while vortexing. This mixture was held on ice and further emulsified with an immersion probe sonicator (TMX 400, Tekmar, Cincinnati, OH) with three, 15 s duration pulses at 40% amplitude. Nanoparticles were added to 100 mL of dilute PVA (0.3%) to allow the solvent to evaporate. Hardened nanoparticles were collected by centrifugation, washed, size-fractionated by centrifugation, and lyophilized with a cryoprotectant (0.5 mg trehalose per 1 mg PLGA). Nanoparticle size and morphology were assessed with scanning electron microscopy (SEM).

Synthesis and Characterization of [^{18}F]NPB4 Labeled Nanoparticles. Conjugation of [^{18}F]NPB4 with avidin surface coated PLGA nanoparticles followed procedure similar to that described above for the reaction of [^{18}F]NPB4 with avidin. In brief, 20 mg of small (∼70 nm) or large size (∼150 nm) PLGA nanoparticles was added to approximately 1 mCi of [^{18}F]NPB4 in 0.5 mL of PBS. The resulted suspension was incubated for 30 min at room temperature and sonicated for 5 min before injection to animals.

To test the efficiency of [^{18}F]NPB4 conjugation to nanoparticles, the radiolabel was incubated with large nanoparticles for 30 min followed by centrifugation for 10 min at 10 000 *g*. The supernatant was removed, and the precipitate was washed and the solution was combined with the supernatant. Radioactivity in the supernatant and precipitate was measured, and compared to the total radioactivity added. Supernatant radioactivity was no higher than background levels.

Imaging. All animal procedures were carried out under a protocol approved by the Yale University Institutional Animal Care and Use Committee. Male Sprague−Dawley rats (250−350 g, Charles River Laboratory) were anesthetized for surgery with an intraperitoneal injection of ketamine/xylazine (90/10 mg/kg, Henry Schein). A 26 G guide cannula (Plastics One, Roanoke, VA) was lowered onto the top of the skull to target the striatum (3.8 mm posterior, 2.1 mm lateral, and 4.0 mm ventral from bregma). Three stainless steel cranial screws were placed within 1 cm of the guide cannula and cemented into place with a fast curing resin (Perm Reline, Henry Schein). Imaging sessions began approximately 1−2 h after initial anesthesia induction, and rats were maintained on 2% isoflurane for the scan duration. Polyethylene tubing attached to a 28 G injector (Plastics One) with a projection to target −6.0 mm DV was primed with nanoparticle solution and attached to a 50 μL Hamilton syringe containing saline. Injections were performed with the aid of an automated syringe pump (Harvard PHD 22/2000 Advance Syringe Pump, Harvard Apparatus, Holliston, MA).

Data were acquired with a FOCUS 220 small animal PET scanner (Siemens Medical Solutions, Knoxville, TN). A 9 min transmission scan (^{57}Co source) was acquired to correct for attenuation. List mode data were collected during the infusion and for up to 2 h thereafter. Data were binned into 0.5 to 10 min frames, which were reconstructed with the ordered subset expectation maximization (OSEM, 4 iterations with 16 subsets) algorithms with corrections for decay, attenuation, randoms, and scatter. Image resolution was ∼1.5 mm, with a pixel size of 0.949 × 0.949 × 0.796 mm^3.

Data Analysis. The center of the infusion was identified on coronal sections of each time series at the beginning and end of each infusion. These coordinates were compared to the transmission image to ensure the injector reached the target location of ∼6 mm ventral to bregma. Three-dimensional data were cropped to ±10 pixels from the center of the infusion, yielding a total volume of 21 × 21 × 21 pixels for each time frame. Total radioactivity delivered was measured by summing pixel values across this volume. The fraction of the total radioactivity delivered was calculated by dividing the total radioactivity signal in that frame by the total radioactivity signal at the end of the 30 min infusion. These data are expressed as "delivered fraction" with a maximum value of 1. To measure a spatial volume of distribution, pixel values were compared to a threshold value (1%, 2%, 3%, 5%, or 10% of the maximum concentration in the frame), and the total volume above threshold was calculated by converting the number of voxels to cm^3. A threshold value of 2% was observed to produce the most consistent volume measurements (judging by the lowest variation in final volume of distribution measured for different subjects) and thus was chosen as the threshold value for the data shown here. Data were collected for 6 nanoparticle infusions (n = 4 for small nanoparticles, and n = 2 for large nanoparticles). One of the small nanoparticle infusions experienced backflow, where some of the infusate was driven back up along the catheter track. These data were excluded from the spatial volume of distribution analysis. Since clearance rates, measured from the region directly surrounding the

catheter tip, are unaffected by backflow, these data were included in the nanoparticle clearance calculation.

AUTHOR INFORMATION

Corresponding Author

*E-mail: henry.huang@yale.edu. Telephone: 203-785-3193. Fax: 203-785-2994.

Author Contributions

Rachael W. Sirianni and Ming-Qiang Zheng contributed equally to this work.

Notes

The authors declare no competing financial interest.

ACKNOWLEDGMENTS

The authors gratefully acknowledge the contributions of the staff of the Yale PET Center, including Maria Corsi, Krista Fowles, Jim Ropchan, Patrick Ouellette, and Nancy Nishimura for their technical assistance. The authors also acknowledge Songye Li, Justin Sciuto for the melting point and ^{1}H NMR analysis, and Edward Voss for the HRMS analysis. This work was supported by National Institutes of Health grants, T32DA022975 ("Neuroimaging Sciences Training Program") and CA149128, and was also made possible by CTSA Grant Number UL1RR024139 from the National Center for Research Resources (NCRR) and the National Center for Advancing Translational Science (NCATS), components of the National Institutes of Health (NIH), and NIH roadmap for Medical Research. Its contents are solely the responsibility of the authors and do not necessarily represent the official view of NIH.

ABBREVIATIONS

CED, convection enhanced delivery; ECM, extracellular matrix; NPB4, Fluorobenzylamide-poly(ethylene glycol)$_4$-biotin; PBS, phosphate buffered saline; PEG, poly(ethylene glycol); PET, positron emission tomography; PLGA, poly(lactic-*co*-glycolic acid); SPECT, single photon emission computed tomography

REFERENCES

(1) Diamandis, E. P., and Christopoulos, T. K. (1991) The biotin-(strept)avidin system: principles and applications in biotechnology. *Clin. Chem. 37*, 625−36.

(2) Fahmy, T. M., Samstein, R. M., Harness, C. C., and Mark Saltzman, W. (2005) Surface modification of biodegradable polyesters with fatty acid conjugates for improved drug targeting. *Biomaterials 26*, 5727−36.

(3) Zhou, J., Patel, T. R., Fu, M., Bertram, J. P., and Saltzman, W. M. (2012) Octa-functional PLGA nanoparticles for targeted and efficient siRNA delivery to tumors. *Biomaterials 33*, 583−91.

(4) Susumu, K., Mei, B. C., and Mattoussi, H. (2009) Multifunctional ligands based on dihydrolipoic acid and polyethylene glycol to promote biocompatibility of quantum dots. *Nat. Protoc. 4*, 424−36.

(5) Park, J., Mattessich, T., Jay, S. M., Agawu, A., Saltzman, W. M., and Fahmy, T. M. (2011) Enhancement of surface ligand display on PLGA nanoparticles with amphiphilic ligand conjugates. *J. Controlled Release 156*, 109−15.

(6) Park, J., Fong, P. M., Lu, J., Russell, K. S., Booth, C. J., Saltzman, W. M., and Fahmy, T. M. (2009) PEGylated PLGA nanoparticles for the improved delivery of doxorubicin. *Nanomedicine: Nanotechnology, Biology, and Medicine 5*, 410−8.

(7) Cu, Y., and Saltzman, W. M. (2009) Controlled surface modification with poly(ethylene)glycol enhances diffusion of PLGA nanoparticles in human cervical mucus. *Mol. Pharmaceutics 6*, 173−81.

(8) Zhou, J., Patel, T. R., Sirianni, R. W., Strohbehn, G., Zheng, M. Q., Duong, N., Schafbauer, T., Huttner, A. J., Huang, Y., Carson, R. E., Zhang, Y., Sullivan, D. J., Jr., Piepmeier, J. M., and Saltzman, W. M. (2013) Highly penetrative, drug-loaded nanocarriers improve treatment of glioblastoma. *Proc. Natl. Acad. Sci. U. S. A. 110*, 11751−6.

(9) Allard, E., Passirani, C., and Benoit, J. P. (2009) Convection-enhanced delivery of nanocarriers for the treatment of brain tumors. *Biomaterials 30*, 2302−18.

(10) Locatelli, E., Naddaka, M., Uboldi, C., Loudos, G., Fragogeorgi, E., Molinari, V., Pucci, A., Tsotakos, T., Psimadas, D., Ponti, J., and Franchini, M. C. (2014) Targeted delivery of silver nanoparticles and alisertib: in vitro and in vivo synergistic effect against glioblastoma. *Nanomedicine (Lond.) 9*, 839−849.

(11) Mok, H., Veiseh, O., Fang, C., Kievit, F. M., Wang, F. Y., Park, J. O., and Zhang, M. (2010) pH-Sensitive siRNA nanovector for targeted gene silencing and cytotoxic effect in cancer cells. *Mol. Pharmaceutics 7*, 1930−9.

(12) Fogarasi, M., Pullman, J., Winnard, P., Jr., Hnatowich, D. J., and Rusckowski, M. (1999) Pretargeting of bacterial endocarditis in rats with streptavidin and ^{111}In-labeled biotin. *J. Nucl. Med. 40*, 484−90.

(13) Urbano, N., Papi, S., Ginanneschi, M., De Santis, R., Pace, S., Lindstedt, R., Ferrari, L., Choi, S., Paganelli, G., and Chinol, M. (2007) Evaluation of a new biotin-DOTA conjugate for pretargeted antibody-guided radioimmunotherapy (PAGRIT). *Eur. J. Nucl. Med. Mol. Imaging 34*, 68−77.

(14) Blom, E., Langstrom, B., and Velikyan, I. (2009) ^{68}Ga-labeling of biotin analogues and their characterization. *Bioconjugate Chem. 20*, 1146−51.

(15) Bolzati, C., Caporale, A., Agostini, S., Carta, D., Cavazza-Ceccato, M., Refosco, F., Tisato, F., Schievano, E., and Bandoli, G. (2007) Avidin-biotin system: a small library of cysteine biotinylated derivatives designed for the $[^{99m}Tc(N)(PNP)]^{2+}$ metal fragment. *Nucl. Med. Biol. 34*, 511−22.

(16) Garg, P. K., Garg, S., Degraff, W. G., Zalutsky, M. R., and Mitchell, J. B. (1992) 4-Fluorobenzylamine and phenylalanine methyl ester conjugates of 2-nitroimidazole: evaluation as hypoxic cell radiosensitizers. *Int. J. Radiat. Oncol. Biol. Phys. 22*, 593−6.

(17) Haradahira, T., Hasegawa, Y., Furuta, K., Suzuki, M., Watanabe, Y., and Suzuki, K. (1998) Synthesis of a F-18 labeled analog of antitumor prostaglandin delta 7-PGA1 methyl ester using *p*-[^{18}F]-fluorobenzylamine. *Appl. Radiat. Isot. 49*, 1551−6.

(18) Leung, K. (2004) [^{18}F]alpha/gamma-Fluorobenzylamine-folate, in *Molecular Imaging and Contrast Agent Database (MICAD)*; Bethesda, MD.

(19) Zhang, H., Huang, R., Pillarsetty, N., Thorek, D. L., Vaidyanathan, G., Serganova, I., Blasberg, R. G., and Lewis, J. S. (2014) Synthesis and evaluation of ^{18}F-labeled benzylguanidine analogs for targeting the human norepinephrine transporter. *Eur. J. Nucl. Med. Mol. Imaging 41*, 322−32.

(20) Way, J., and Wuest, F. (2013) Fully automated synthesis of 4-[^{18}F]fluorobenzylamine based on borohydride/$NiCl_2$ reduction. *Nucl. Med. Biol. 40*, 430−6.

(21) Liu, G., Mang'era, K., Liu, N., Gupta, S., Rusckowski, M., and Hnatowich, D. J. (2002) Tumor pretargeting in mice using ^{99m}Tc-labeled morpholino, a DNA analog. *J. Nucl. Med. 43*, 384−91.

(22) Sirianni, R. W., Zheng, M. Q., Saltzman, W. M., Huang, Y., and Carson, R. E. (2013) Direct, quantitative, and noninvasive imaging of the transport of active agents through intact brain with positron emission tomography. *Mol. Imaging Biol. 15*, 596−605.

(23) Najafi, A., and Peterson, A. (1993) Preparation and in vitro evaluation of "no-carrier-added" ^{18}F-labeled biotin. *Nucl. Med. Biol. 20*, 401−5.

(24) Shoup, T. M., Fischman, A. J., Jaywook, S., Babich, J. W., Strauss, H. W., and Elmaleh, D. R. (1994) Synthesis of fluorine-18-labeled biotin derivatives: biodistribution and infection localization. *J. Nucl. Med. 35*, 1685−90.

(25) Ting, R., Harwig, C., auf dem Keller, U., McCormick, S., Austin, P., Overall, C. M., Adam, M. J., Ruth, T. J., and Perrin, D. M. (2008) Toward [^{18}F]-labeled aryltrifluoroborate radiotracers: in vivo positron

emission tomography imaging of stable aryltrifluoroborate clearance in mice. *J. Am. Chem. Soc. 130*, 12045−55.
(26) Karp, J., and Zhao, W. (2014) in *Micro and Nano Technologies*; Elsevier.
(27) Lee, T. K., O'Brien, K. F., Wang, W., Sheng, C., Wang, T., Johnke, R. M., and Allison, R. R. (2009) American ginseng modifies Cs-induced DNA damage and oxidative stress in human lymphocytes. *Open Nucl. Med. J. 1*, 1−8.
(28) Petronzelli, F., Pelliccia, A., Anastasi, A. M., Lindstedt, R., Manganello, S., Ferrari, L. E., Albertoni, C., Leoni, B., Rosi, A., D'Alessio, V., Deiana, K., Paganelli, G., and De Santis, R. (2010) Therapeutic use of avidin is not hampered by antiavidin antibodies in humans. *Cancer. Biother. Radiopharm. 25*, 563−70.
(29) Song, X., and Swanson, B. I. (2002) Ultrasensitive and Specific Optical Biosensors Inspired by Nature, in *Diagnostic Science and Technology* (Law, W. T., Akmal, N., and Usmani, A. M., Eds.) pp 165−186, Marcel Dekker, Inc.
(30) Nakamura, K., Wang, Y., Liu, X., Kubo, A., and Hnatowich, D. J. (2007) Cell culture and xenograft-bearing animal studies of radiolabeled antisense DNA carrier nanoparticles with streptavidin as a linker. *J. Nucl. Med. 48*, 1845−52.
(31) Mock, D. M., and DuBois, D. B. (1986) A sequential, solid-phase assay for biotin in physiologic fluids that correlates with expected biotin status. *Anal. Biochem. 153*, 272−8.
(32) Haka, M. S., Kilbourn, M. R., Watkins, G. L., and Toorongian, S. A. (1989) Aryltrimethylammonium trifluoromethanesulfonates as precursors to aryl [^{18}F]fluorides: Improved synthesis of [^{18}F]GBR-13119. *J. Labelled Compd. Radiopharm. 27*, 823−833.
(33) McCall, R. L., and Sirianni, R. W. (2013) PLGA nanoparticles formed by single- or double-emulsion with vitamin E-TPGS. *J. Visualized Exp. 27* (e51015), 1−8.